A Novel Porous Graphene Scaffold Prepared Using Freeze-Drying Technique for Orthopedic Approaches: Fabrication and Buckling Simulation Using GDQ Method

S. Foroutan, M. Hashemian* and A. S. Khandan

* hashemian@iaukhsh.ac.ir

* Department of Mechanical Engineering, Khomeinishahr Branch, Islamic Azad University, Khomeinishahr, Iran

Abstract: In this article, a novel bio-nanocomposite sample made of sodium alginate polymer, graphene nano-sheets and wollastonite powder were produced using freeze-drying technique. The samples were mechanically and biologically evaluated using tensile strength and biological test. The phase and topological characterization were conducted by performing X-ray diffraction (XRD) and scanning electron microscopy (SEM) studies. Subsequently, using Euler-Bernoulli and Timoshenko beam (EBT and TBT) theories, the buckling response of the porous bio-nanocomposite soft tissue were analyzed with respect to graphene content. In order to solve the governing equations a sufficient numerical solution is proposed. Elastic modulus and mass density of the porous bio-nanocomposite are extracted from the experimental tests. The obtained results indicated the sample with 1 wt.% graphene sheet showed proper mechanical and biological features. Therefore, the sample with 1 wt.% graphene sheet can be used as potential case for light weight bone substitute applications.

Keywords: Scaffold, Graphene, Buckling analysis, Freeze-drying, Wollastonite.

1. INTRODUCTION

Regarding human body disability of repairing bone defects, application of artificial bone tissue has received much attention in recent decades. New generation of bio-scaffolds are the appropriate approach for defective bone tissue. Bone defects are the consequences arising from trauma, accident, genetic or disease [1]. Recently, several studies have been conducted to produce novel porous bio-nanocomposite scaffold materials using various methods for clinical applications [2-4]. Biomaterials used in this category of application should be bioactive and made of synthetic or natural polymers, ceramics, and metals with sufficient porosity to ensure blood circulation inside human body using software and anatomical model [5-10]. Despite bioactivity, such materials have shown low mechanical properties and weak chemical stability beside problematic reaction in biological environment. Sufficient techniques have been presented to improve biomaterial mechanical characteristics such as compressive strength, fracture toughness, porosity and tensile strength [11-16]. Ceramic materials including hydroxyapatite (HA), biphasic calcium phosphate (CaP), bio-glasses (BG), and β-

tricalcium phosphate (βTCP) are being employed in bone tissue engineering applications [17-25]. Moreover, calcium silicates (CS), as a class of glass silicate, are one the bio-active-ceramic that has been utilized for orthopedic applications for decades [26-27]. The CS bioceramics are also used as coating cover for improving bioactivity of the porous scaffold implants [27]. Another fascinating property of CS is the ability to bond with natural bone inside the body, and the combination of CS with Magnesium (Mg) [28], Zinc (Zn), Strontium (Sr) [29] results in ameliorate molecular bonding properties for bone tissue approaches [30]. The CS bioceramic perform better mechanical behavior in comparison to other CaP bio-ceramics [31]. However, due to the required porosity and proper porous microarchitecture, the scaffold discloses unsuitable mechanical stiffness required for body weight and applied forces. Xu et al. [32] conducted in vivo bone-generative resorption and evaluate the capacity of porous bioactive β-calcium silicate (β-CS) ceramics in a rabbit calvarial defect model. The β-CS ceramic was implanted in rabbit calvarial defect for 4, 8, and 16 weeks. Lin et al. [33] scrutinized the osteoporotic defect bone generation improvements by utilizing porous Sr-

substituted calcium ceramic scaffolds. Improving the mechanical characteristic of CS has been a controversial topic since the first usage of this material in biomedical application. Several strategies are proposed for improving its mechanical performance including reinforcement like graphene sheet (GS), magnetite nanoparticles (MNPs) or carbon nanotubes (CNTs). Mehrali et al. [34] synthesized a calcium silicate-reduced graphene oxide for hard tissue applications with enhanced mechanical properties using graphene reinforced CS. GS and CS both indicated proper biocompatibility features for bone microstructures like scaffolds and porous network. Shao et al. [35] developed a high strength Mg-doping wollastonite based scaffold by 3D printing technology having pore size and the heating procedure to strengthen the scaffold microstructure. Several polymers have been used for such purpose including chitosan, alginate, sodium alginate, gelatin application in pharmacokinetics [36-42, 53]. Xiong et al. [43] proposed a novel hybrid sodium alginate-based nanocomposite reinforce via graphene oxide and hydroxyapatite produced by freeze-drying method to mimic required mechanical and biological properties range. Another application of hybrid tissue is water treatment, for instance, Karkeh-abadi et al. [44] developed efficient adsorbents to remove radioactive pollutants from medical and industrial wastewater by functionalized CNT in sodium alginate-based nanocomposite. Lonita et al. [45] presented a novel study on the sodium alginate graphene oxide nanocomposite films with enhanced mechanical and thermal properties showing high interfacial adhesion between graphene and alginate matrix due to its hydrogen boding remarkably altered the mechanical properties and thermal stability of the bio-nanocomposite films. Scaffold fabrication techniques including solvent casting [46], particulate-leaching [47], gas foaming [48], phase separation [49], freeze-drying [50-51], and 3D printing [52-53] are being used widely for biomedical usage. However, among these techniques, freeze-drying is one of the important, low cost, easily accessible and developed methods since it has the ability to control the porosity by the rate of freezing. Khorsand et al. [53] developed TiO_2 based scaffold doped in chitosan/HA utilizing freeze drying technique with various hydroxyapatite ratios. The application bio-nanocomposites are extended in term of other fields studies including dental application [54-58]. In previous study, Foroutan et al. [59] concentrated on manufacturing polymer-based scaffold with wollastonite-graphene reinforcement. The mechanical and biological characterizations of prepared scaffold are studied. Moreover, the optimization is applied to the study for clear announcement of the optimum sample. Saber-Samandari et al. [60] prepared polyacrylamide-based nanocomposite scaffold incorporating nanohydroxyapatite by freeze drying method. To evaluate the mechanical behavior of the prepared bio-nanocomposite, the Timoshenko and Euler-Bernoulli beam theories are applied in different studies to investigate the buckling and bending behavior of beams. Sahmani et al. [61] investigated the nonlinear bending and instability of bredigite bioceramic incorporating magnetic nanoparticle. Foroutan et al. [62] proposed the buckling behavior analysis of current carrying nanowires regarding the magnetic field (MF) effects incorporating surface and nonlocal effects. Results revealed the MF increases the buckling load while nonlocal parameter reduces the buckling load. The mechanical and biological feature of biomaterials domain has been investigated with various techniques such as wet chemistry and mechanical activation methods. Several works have been conducted on drug loading and effect of nanoparticles on the composite. Molecular dynamic (MD) evaluation also can predict the mechanical properties of macron and micron scale [63-77]. Various numerical investigation has been performed on the composite to discover the influence of interphase of composite mathematically [68-74]. In the current paper, the sodium alginate biopolymer is composed with wollastonite ceramic to prepare proper bone substitution for orthopedic approaches. Moreover, GS is added in various content levels to the bio-nanocomposite. Mechanical and biological characterizations of the prepared bio-nanocomposite are surveyed. In order to investigate the mechanical behavior of the composed bio-nanocomposite, the Timoshenko and Euler-Bernoulli Beam theories (TBT) and (EBT) are used based upon the extracted elastic

modulus and mass density of the porous bio-nanocomposite from experimental examination to develop the classical beam responses.

2. EXPERIMENTAL PROCEDURES

2.1. Raw Materials
In the current study, the graphene nanosheet was used to enhance the new generation of calcium silicate (CS) scaffold. Sodium alginate (SA) as a natural polymer (Mw=216.12 g/mol, 98% purity, size <100 nm Merck company, Germany) were purchased. The wollastonite nanopowder was fabricated using high-energy ball milling (HEBM) and graphene sheet (GS) nanoplatelets (US Research Nanomaterials, Inc, +99.5%, 2.18 nm with 32 layers) are utilized.

2.2. Wollastonite Preparation
First, the preparation of wollastonite (WS) made of $CaCO_3$ and SiO_2 mixing by magnetic stirrer with 400 rpm and 25 ˚C dissolving in Acetic acid and water solution. Then the obtained gel is kept for 3 days in 70 ˚C. Furthermore, the temperature was increased to 150 ˚C for 24 h to dry the gel [59]. Dried gel is milled and filtered to reach particle size of 10-50 μm. Finally, two heating operation is applied on the particle in 700 ˚C and 1000 ˚C for 3 h to create the WS ceramic powder.

2.3. Nanocomposite Preparation
After the WS was prepared, manufacturing process of scaffold composites was performed. Briefly, 7.5 gr of sodium alginate powder was synthesized with 100 mL distilled water and 1 vol% acetic acid stirring for 3h and 1200 rpm with 50 ˚C. After that, 1.8 gr of WS powder were mixed with for various content of graphene (0, 1, 2, and 3 wt% GS) based on constant WS powder. In order to combine the prepared SA biopolymer and synthesized GS-WS powders the digital ultrasonic device is employed [59].

2.4. Scaffold Preparation
Then, the four porous bio-nanocomposite scaffolds were placed into freezer at -70 ˚C for 24 h. The frozen porous scaffold was set into the freeze-drier device for another 24 h at -45 ˚C with 0.01 bar to drain all the available waters to improvise required porosity (DORSA-TECH Company, Tehran, Iran) [59]. Porous scaffold removed from the freeze-drier machine after 48 h and placed in the incubator. Therewith, the

mechanical and biological tests are performed on the four porous bio-nanocomposites.

2.5. Characterization

2.5.1. Porosity Measurement
To evaluate the porosity of the bio-nanocomposite, the Archimedes and Image-J techniques were used. To this end, a graded cylindrical container with a fixed stilled water volume (V_1) is utilized [59]. Then, the prepared bio-nanocomposite was place into the water so that the water penetrates all the available porosity in the matter (V_2). Afterward, the composite was pulled out of the container and the volume of water was measured (V_3). The formula for the porosity percentage is written as equation 1:

$$Porosity\ (\%) = (V_1 - V_3)/(V_2 - V_3) \times 100 \qquad (1)$$

2.5.2. Tensile Strength Evaluation
The mechanical properties of the nanostructure including tensile strength and elastic modulus are investigated by the tensile strength device (SANTAM-STM50) by applying load of 0.5 mm/min [59]. The porous samples are cut into pieces with 9 mm diameter and 20 mm length corresponding to the fixed materials (WS-SA) and various content of GS powder. Obtained data are used to plot the stress-strain graph. The graph slop and the maximum value of stress are the elastic modulus and tensile strength, respectively.

2.6. Biological Evaluation
The Simulated Body Fluid (SBF) was utilized in order to evaluate the pH behavior of bio-nanocomposite. The ionic concentration of SBF is very similar to human blood plasma; therefore, it is used to evaluate the bio-nanocomposite pH behavior. To this end, the samples are drowned in SBF for 1, 3, 7, 14, 21 and 28-day's periods. The pH value is determined using a digital pH meter device at Amirkabir University Technology.

2.7. Microstructural and Phase Characterization
The morphology and structural properties of Na-alginate-WS-Graphene Sheet porous bio-nanocomposite scaffold are characterized through scanning electron microscopy (SEM) at Amirkabir University of technology (SERON Technology-AIS2100, South Korea, Display Magnitude 15 to 30000, Resolution 5/3 nm). The

device voltage and electricity current were 40 KV and 30 mA, respectively. Moreover, phase composition of Na-alginate-WS-GS scaffold is investigated utilizing X-ray diffraction (XRD)

(INEL-EQUNIX 3000, French). Figure 1 displays the manufacturing process of fabricated scaffold bio-nanocomposite and required analysis of the structural characteristics.
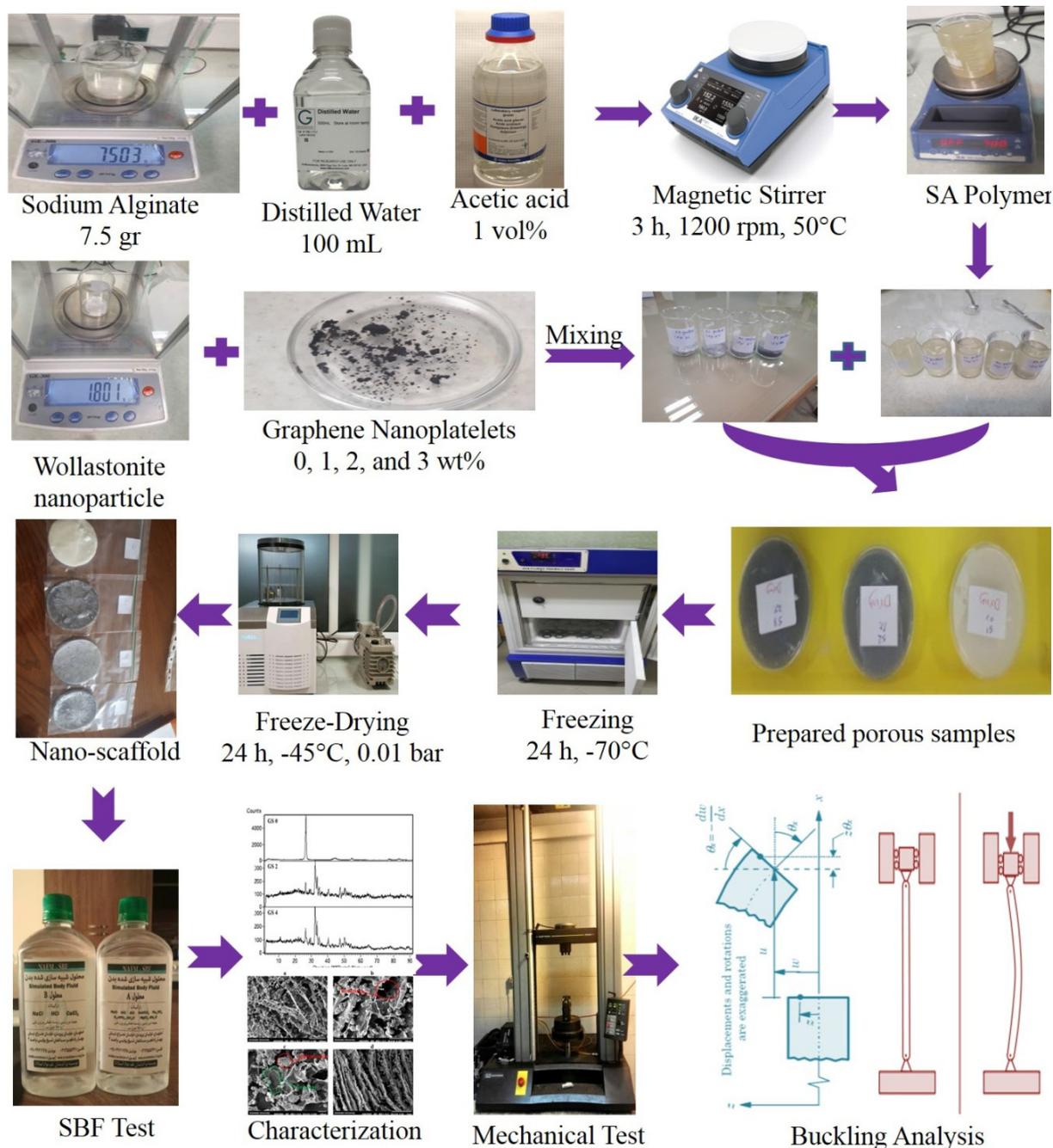
Fig. 1. Schematic of fabrication procedure of porous bio-nanocomposite made of Na-alginate-WS-reinforced with graphene oxide using freeze drying technique.

2.8. Analysis of Porous Scaffold Based on EBT and TBT Theories

In this section, the buckling behavior of bio-nanocomposite is investigated using TBT and EBT. Governing equations are derived based on both Euler-Bernoulli (EBT) and Timoshenko Beam Theories (TBT). Clamp-clamp (C-C) boundary conditions are imposed to simulate the bone replacement in the human body. Afterwards, the governing equations are solved using Generalized Differential Quadrature Method (GDQM) [12, 62 and 64]. According to the Hamilton's principle the buckling equilibrium equations is written as:

$$\delta U - \delta W = 0$$

Where δU and δW are virtual strain energy and virtual work done by external applied forces, respectively. Regarding the EBT and TBT theories, displacement fields are expressed as:

$$u(x,z) = u(x) - z\frac{dw(x)}{dx} + P(z)\left[\frac{dw(x)}{dx} - \varphi(x)\right], \quad (2)$$

$$v(x,z) = 0,$$

$$w(x,z)w(x),$$

Where u, w, and φ are axial displacements, transverse displacements, and angle rotation of cross section about y-axis, respectively. P(z) for both EBT and TBT is defined as:

$$P(z) = 0 \qquad \text{EBT}$$

$$P(z) = z \qquad \text{TBT} \qquad (3)$$

Based on defined displacement field, the strain components can be express as:

$$\varepsilon_{xx} = \frac{du}{dx} - P\frac{d\varphi}{dx} - (z-P)\frac{d^2w}{dx^2}, \qquad (4)$$

$$\varepsilon_{xz} = \frac{1}{2}\frac{dP}{dz}\left(\frac{dw}{dx} - \phi\right)$$

In order to derive the classical governing equations based on Hamilton's principle, the stress resultants are defined as:

$$\left\{\hat{N}, \hat{M}, \hat{H}\right\} = \int_A \sigma_{xx}\{1, P, (z-P)\}dA, \hat{Q} = \int_A \sigma_{xz}\frac{dP}{dz}dA, (5)$$

Where σ_{xx} and σ_{xz} denote stress tensor components. Finally, the generalized governing equations (GGE) are derived according Hamilton's principle as follow:

$$\delta u : \frac{d\hat{N}}{dx} + f = 0, \qquad (6)$$

$$\delta w : \frac{d^2\hat{H}}{dx^2} + \frac{d\hat{Q}}{dx} + q - \frac{d}{dx}\left(N_m\frac{dw}{dx}\right) = 0,$$

$$\delta\varphi : \frac{d\hat{M}}{dx} - \hat{Q} = 0$$

Where $\delta\varphi$ is merely expressed in TBT. Moreover, q and f are the transverse and distributed axial loads, respectively. For EBT and TBT the derived equations based on Eq. 5 are written as:

$$\delta w : EI\frac{d^4w}{dx^4} - N_m\frac{d^2w}{dx^2} = 0, \qquad \text{EBT} \quad (7)$$

$$\delta u : EA\frac{d^2u}{dx^2} = 0, \qquad (8)$$

$$\delta w : GA\left(\frac{d^2w}{dx^2} - \frac{d^2}{dx^2}\right) - N_m\frac{d^2w}{dx^2} = 0, \quad \text{TBT}$$

$$\delta\varphi : -EI\frac{d^2\varphi}{dx^2} - GA\left(\frac{dw}{dx} - \right) = 0,$$

Where G is the shear modulus of elasticity that can be derived from $G = E/(2(1+\nu))$, ν is the Poisson's ratio which can be derived from rule of mixture (ROM) as [65]:

$$\nu = \nu_{Ws}V_{ws} + \nu_{SA}V_{SA} + \nu_{Gr}V_{Gr},$$

Where V_{ws}, V_{SA}, and V_{Gr} are the volume fraction WS, SA, and GS, respectively. Moreover ν_{Ws}, ν_{SA}, and ν_{Gr} are the Poisson's ratios for WS, SA and GS, respectively. For acquiring more general responses the following dimensionless groups are utilized:

$$x^* = \frac{x}{L}, w^* = \frac{w}{L}, \varphi^* = \varphi, \beta = \frac{N_mL^2}{EI} \qquad \text{EBT}$$

$$\alpha = \frac{I}{AL^2}, \psi = \frac{G}{E}, \gamma = \frac{N_m}{EA} \qquad \text{TBT} \qquad (9)$$

2.8.1. Generalized Differential Quadrature Method (GDQM)

In order to solve the derived equation a numerical method is used. This method is known as Generalized Differential Quadrature Method (GDQM) [59-64] which is famous for its simple and low-cost calculations. Applying the boundary conditions is an outstanding point of this method since the boundary conditions can

be imposed simultaneously with the calculations. There are no restrictions on the number of mesh points applied for approximation in this method. Moreover, the weighted coefficients are derived by simple recurrence relation rather than a set of algebraic equations. These two advantages make GDQM a superior method in comparison to other DGM approaches [12, 62, 64, 65]. The partial derivations of function f with respect to spatial variables at the point x_i are expressed as:

$$\frac{d^n f}{dx^n} = \sum_{j=1}^{N} C_{ij}^{(n)} f(x_j), \tag{10}$$

where $C_{ij}^{(n)}$ and N are weighted coefficients matrix and the number of mesh points, respectively. Moreover, f can be replaced by u, w, and φ. For the first derivation, weighted coefficient matrix is written as:

$$C_{ij}^{(1)} = \begin{Bmatrix} \prod_{k=1,k\neq i,j}^{N}(x_{i-}x_k) & \prod_{k=1,k\neq j}^{N}(x_i\ x_k) & i \neq j \\ \sum_{k=1,k\neq i}^{N}\frac{1}{(x_i-x_k)} & (i=j) \end{Bmatrix} \tag{11}$$

Where i, j are natural numbers. The weighted coefficient for higher-order derivation is expressed as:

$$C_{ij}^{(2)} = \sum_{k=1}^{N} C_{ik}^{(1)}C_{kj}^{(1)}$$

$$C_{ij}^{(3)} = \sum_{k=1}^{N} C_{ik}^{(2)}C_{kj}^{(1)}$$

$$C_{ij}^{(4)} = \sum_{k=1}^{N} C_{ik}^{(3)}C_{kj}^{(1)} \tag{12}$$

Another important factor in the accuracy and the convergence of the solution is the distribution pattern of the mesh points. Here, the Chebyshev-Gauss-Lobatto (CGL) distribution pattern is expressed as:

$$x_i = \frac{1}{2}\left\{1-\cos\left[\frac{(i-1)\pi}{(N-1)}\right]\right\} \quad i=1, 2, 3,\ldots, N$$

For improving the accuracy of the responses in implementation of GDQ method, the number of mesh points for a converged response are shown in Fig. 2.

2.8.2. Applying the Boundary Conditions

The corrected collocation method [65] is applied to enforce the boundary conditions. For clamp-clamp boundary condition the following

boundary conditions are imposed in the governing equations:

w(0)=w(1)=0

w'(0)=w'(1)=0

w(0)=w(1)=0

u(0)=u(1)=0

φ(0)=φ(1)=0

Solving the equations based on GDQM and the essential boundary condition requires the application of eigenvalue theorem. After implementation of the eigenvalue theorem, the minimum dimensionless critical buckling load is obtained, then by utilizing the related dimensionless term the value of critical buckling load is acquired. The constant geometrical and mechanical values used in this research are assumed as:

L=15mm, D=1.5mm, ν_{Ws}=0.3, ν_{SA}=0.5, ν_{Gr}=0.3
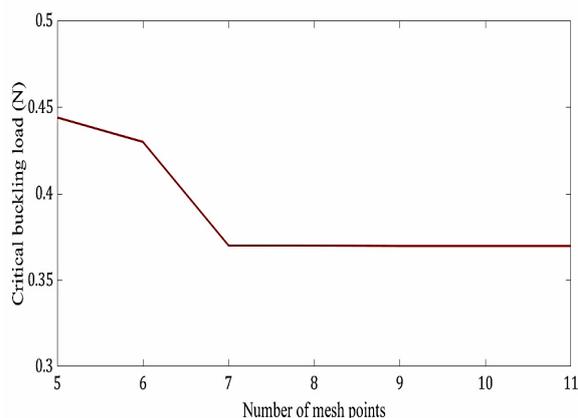

Fig. 2. The critical buckling load in terms of number of mesh point

3. RESULTS AND DISCUSSION

In this section, the obtained results from the biological and mechanical tests are discussed and evaluated thoroughly. Moreover, XRD, SEM, and numerical analysis are debated regarding the obtained results. By the means of such tests and analysis the bio-nanocomposite behavior and bio-compatibility are examined, and the 1 wt% GS is selected as the most sufficient one.

3.1. Mechanical Tests

Fig. 3 depicts the stress-strain graph for four

levels of graphene weight percent. Extracted from the given graph, the elastic modulus is derived. As it is obvious from Fig. 3, increasing the GS weight percent from 0 wt% to 2 wt% would increase the material stiffness. It is absorbing that the GS percentage would decrease the material stiffness for the third level of graphene sheet (GS=3 wt%). This is probably happened due to the mixing features of the materials and agglomeration. Extracted data were obtained from previous work [59] to discover the elastic modulus of 0 to 3 wt% GS added to the sodium alginate-wollastonite.

3.2. pH Observation

In this section the pH behavior of prepared porous bony bio-nanocomposite is discussed. Fig. 4. represents the pH ranges for the basic (without GS) and optimum samples, and this pH rages can influence the rate of degradation. Since, WS is ceramic composed of silicate, it can affect the trend of pH changes and dominate the

trend. Therefore, the basic sample can indicate the trend of pH changes for other various levels of GS powder. It means if the pH basic sample increases the other samples also follows the same trend. However, the GS can also influence the pH ranges. As it is shown in Fig. 4, the WS for pure sample increase the pH value, however; the graphene nanosheet is change reversely.

3.3. XRD Analysis

In this section, the XRD data are analyzed and discussed. Fig. 5 described the XRD reveals that produced bio-nanocomposite are containing GS since the XRD for the pure Gr pick on 26.5° 2θ are repeated for the bio-nanocomposite with 2 and 3 wt% GS. It is also discovered that the picks on approximate 30° are the one showed for the highest pick of WS on almost the same degree. The reasons of such small shifts on the degrees of highest peaks are inferred from the composite structure.
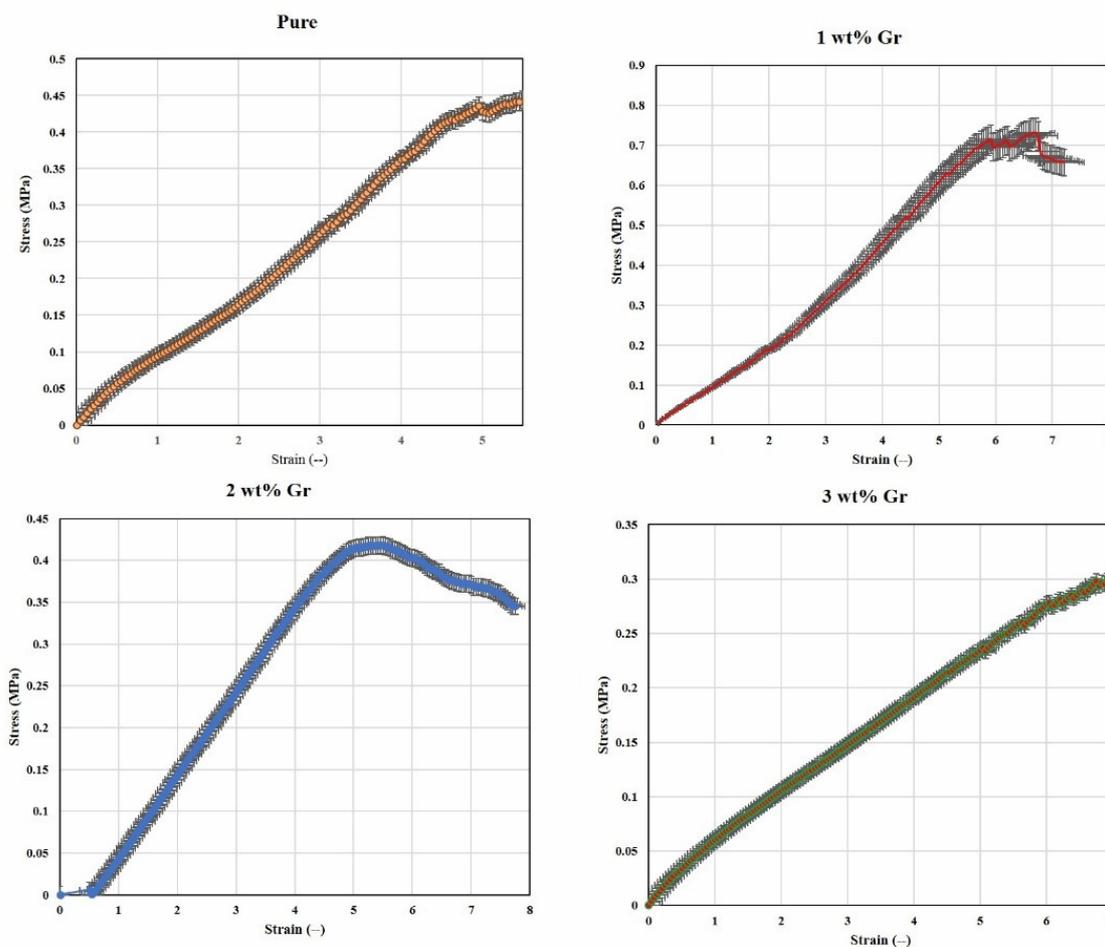

Fig. 3. Stain-stress graph for four levels of Graphene (i.e.; GS= 0-3 wt%)
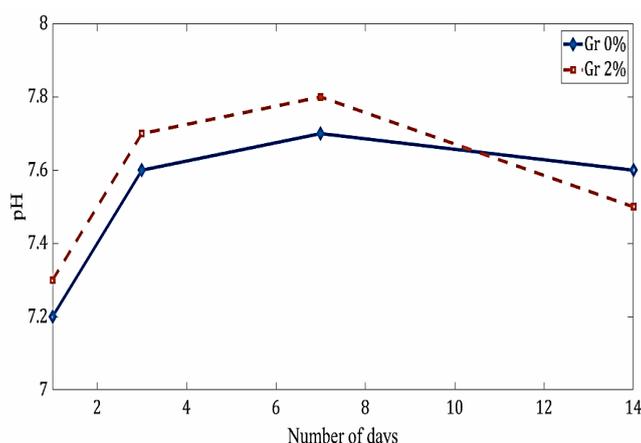
Fig. 4. The pH values in terms of number of days for basic and optimum composites
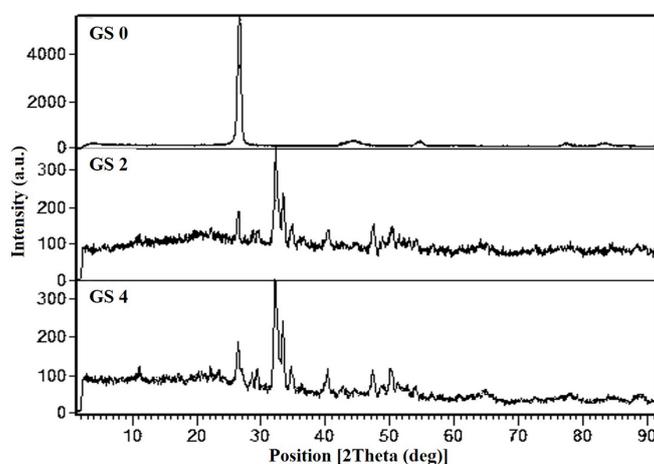
Fig. 5. XRD pattern of prepared scaffold using freeze drying technique containing various amount of GS

3.4. SEM Analysis

The SEM images is a way to see the composite structure including porosity, material, and samples layout. Fig. 6 shows the SEM images of four levels of GS weight percent. Fig. 6(a) shows when GS is not added to the bio-nanocomposite, the bonds between SA and WS are attended to be weak and string like. The WS nanoparticles are clustered and cause to create bio-nanocomposite with low porosity. Moreover, Fig. 6(b) shows the sample with 1 wt% GS chemical bonds between GS and WS are presented, thus the porosity size decrease to the rages of 150-200 μm. Fig. 6(c) displayed that when the GS weight percent increases, the agglomeration happens, and the GS agglomeration bond to the WS nanoparticles. This phenomenon decreases the porosity, but not happening all over the sample. Fig. 6(d) shows the porosities are shaped wall-like, and the connections between WS and GS homogenously distributed all over the sample.

3.5. TBT and EBT Results

In this section, the buckling behavior of bio-nanocomposite beam restricted by clamp-clamp (C-C) boundary condition is discussed, and the obtained results are shown. Fig. 7 introduced the critical buckling load in terms of diameter and length are depicted for four levels of GS based on EBT. As it is previously shown, increasing the diameter incorporate escalations in the values of critical buckling load [12, 59, 62]. In contrast, the length of nanocomposite beam plays a contrariwise role which indicates reduction of critical buckling load as the length grow. Figure 8 plotted the critical buckling load as a function of diameter and length for various levels of GS. Fig. 7 and Fig. 8 displays the same results for length and diameter of bio-nanocomposite. Moreover, increasing the weight percentage of GS in the nanocomposite decreases the material stiffness and diminishes the critical buckling load [66 - 68].

Besides, a comparison of EBT and TBT value in the Figures discloses that the critical buckling load is lower in TBT because of considering more degrees of freedom. After evaluation of TBT and EBT, one can conclude that prepared scaffold compared to the other works have proper

properties to load any drug and consider various nanoparticles in the sodium alginate and wollastonite matrix. Also, application of molecular dynamic (MD) can help the researchers to predict the mechanical properties of macron and micron scale without experimental testing [63-78].
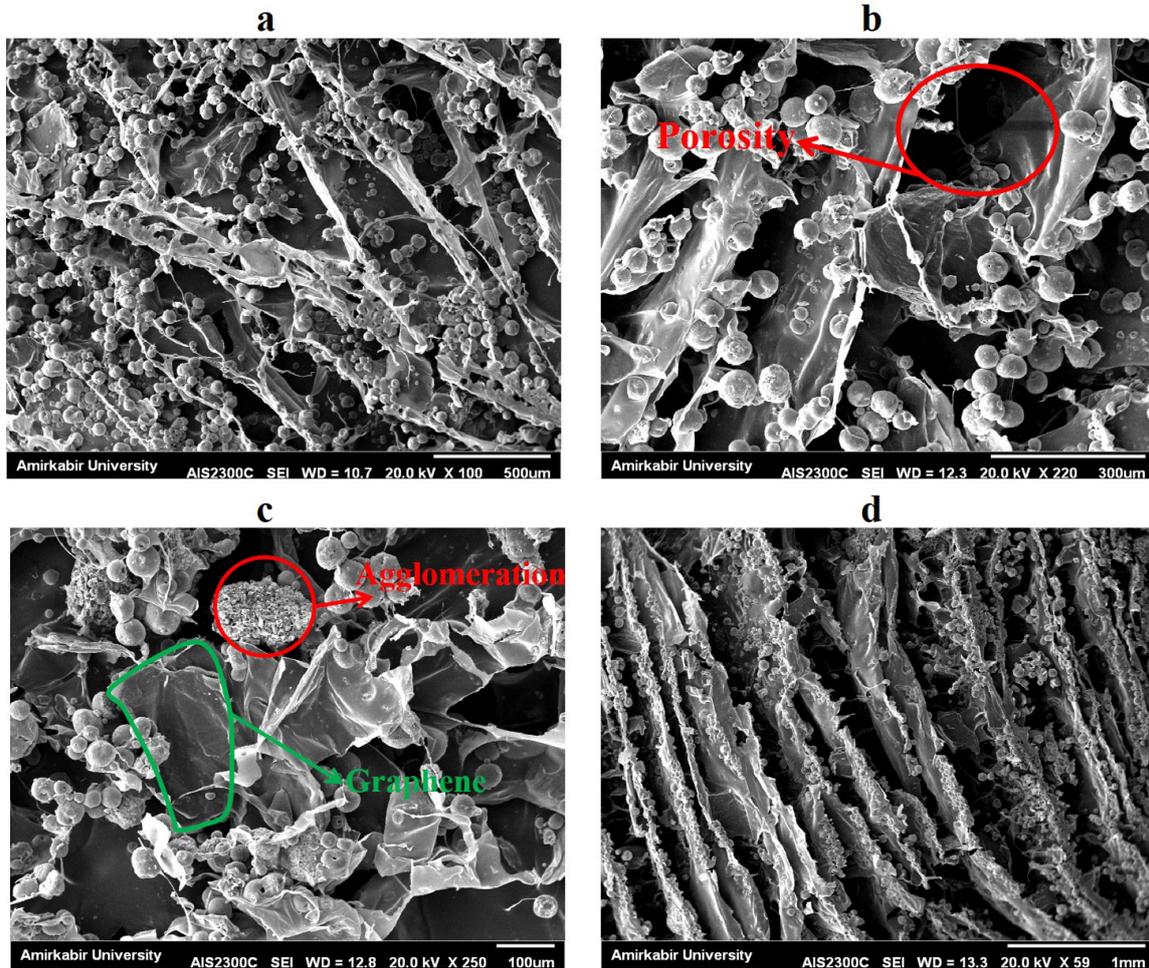
Fig. 6. SEM images of porous sample containing (a) 0 wt%, (b) 1 wt%, (c) 2 wt%, (d) 3 wt% of GS in the sodium alginate-wollastonite matrix fabricated using freeze drying technique
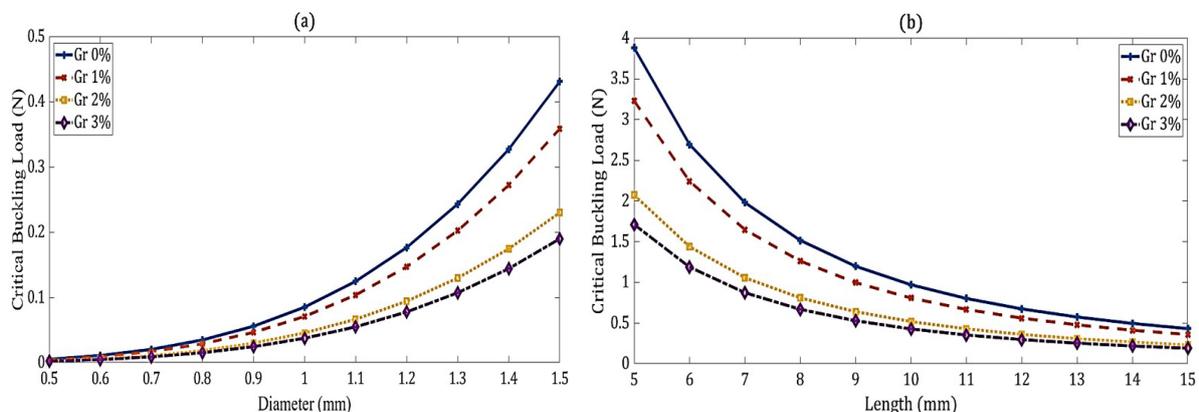
Fig. 7. Variation of critical buckling load in term of nanocomposite (a) diameter, and (b) length for four levels of Graphene based on EBT and clamp-clamp (C-C) boundary condition.
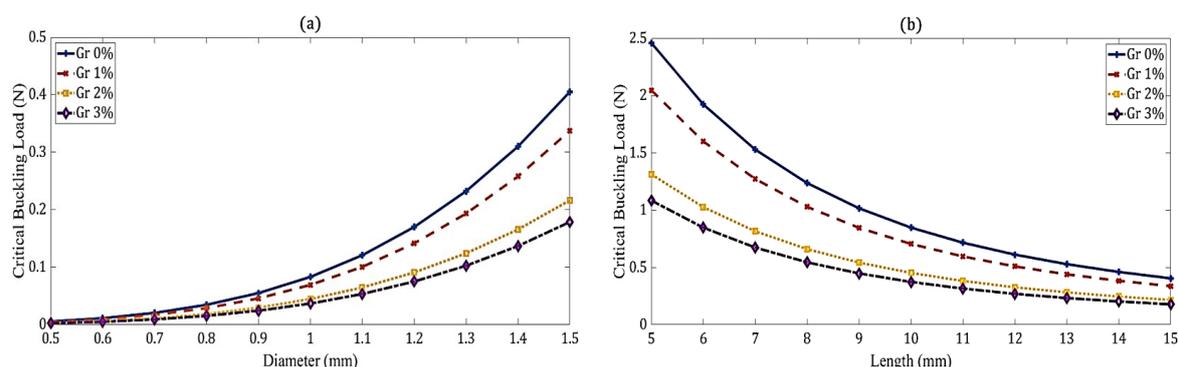
Fig. 8. Variation of critical buckling load in term of nanocomposite (a) diameter, and (b) length for four levels of Graphene based on TBT and clamp-clamp (C-C) boundary condition.

4. CONCLUSION

Elastic modulus and mass density of the bio-nanocomposite are extracted from the experimental tests. The obtained results indicated that the sample with 1 wt. % graphene nanosheet has shown proper mechanical and biological features. Therefore, the sample with 1 wt.% graphene can be used as potential case for light weight bone substitute applications. In this section, the obtained results from the biological and mechanical tests are discussed and evaluated thoroughly. Moreover, XRD, SEM, and numerical analysis are debated regarding the gained images and facts. Using such tests and analysis the bio-nanocomposite behavior and bio-compatibility were examined, and the 1 wt.% graphene nanosheet sample is selected as the most sufficient one. There are no restrictions on the number of mesh points applied for approximation in this method. Moreover, the weighted coefficients are derived by simple recurrence relation rather than a set of algebraic equations. These two advantages make GDQM a superior method in comparison to other DGM approaches. The synthesized calcium silicate-reduced graphene oxide for hard tissue applications with enhanced mechanical properties using graphene nanosheet reinforced CS was successfully achieved.

5. REFERENCES

1. Giannoudis, P. V., Dinopoulos, H., & Tsiridis, E. Bone substitutes: an update. Injury, 2005, 36(3), S20-S27.

2. Farazin, A., Aghdam, H. A., Motififard, M., Aghadavoudi, F., Kordjamshidi, A., Saber-Samandari, S., & Khandan, A. A polycaprolactone bio-nanocomposite bone substitute fabricated for femoral fracture approaches: Molecular dynamic and micro-mechanical Investigation. Journal of Nanoanalysis, 2019, 6(3), 172-184.

3. Khandan, A., Ozada, N., Saber-Samandari, S., & Nejad, M. G. On the mechanical and biological properties of bredigite-magnetite ($Ca_7MgSi_4O_{16}$-Fe_3O_4) nanocomposite scaffolds. Ceramics International, 2018, 44(3), 3141-3148.

4. Monshi, M., Esmaeili, S., Kolooshani, A., Moghadas, B. K., Saber-Samandari, S., & Khandan, A. A novel three-dimensional printing of electroconductive scaffolds for bone cancer therapy application. Nanomedicine Journal, 2020, 7(2), 138-148.

5. Heydary, H. A., Karamian, E., Poorazizi, E., Heydaripour, J., & Khandan, A. Electrospun of polymer/bioceramic nanocomposite as a new soft tissue for biomedical applications. Journal of Asian Ceramic Societies, 2015, 3(4), 417-425.

6. Khandan, A., & Ozada, N. Bredigite-Magnetite ($Ca_7MgSi_4O_{16}$-Fe_3O_4) nanoparticles: A study on their magnetic properties. Journal of Alloys and Compounds, 2017, 726, 729-736.

7. Ghayour, H., Abdellahi, M., Nejad, M. G., Khandan, A., & Saber-Samandari, S. Study of the effect of the Zn^{2+} content on the anisotropy and specific absorption rate of the cobalt ferrite: the application of Co 1− x Zn x Fe_2O_4 ferrite for magnetic hyperthermia. Journal of the Australian Ceramic Society, 2018, 54(2), 223-230.

8. Rad, A. S., Samipour, V., Movaghghar nezhad, S., Mirabi, A., Shahavi, M. H., & Moghadas, B. K. X12N12 (X= Al, B) clusters for protection of vitamin C; molecular modeling investigation. Surfaces and Interfaces, 2019, 15, 30-37.

9. Khandan, A., Jazayeri, H., Fahmy, M. D., & Razavi, M. Hydrogels: Types, structure, properties, and applications. Biomat Tiss Eng, 2017, 4(27), 143-69.

10. Hashemi, S. A., Esmaeili, S., Ghadirinejad, M., Saber-Samandari, S., Sheikhbahaei, E., Kordjamshidi, A., & Khandan, A. Micro-Finite Element Model to Investigate the Mechanical Stimuli in Scaffolds Fabricated via Space Holder Technique for Cancellous Bone. ADMT Journal, 2020, 13(1), 51-58.

11. Iranmanesh, P., Abedian, A., Nasri, N., Ghasemi, E., & Khazaei, S. Stress analysis of different prosthesis materials in implant-supported fixed dental prosthesis using 3D finite element method. Dental Hypotheses, 2014, 5(3), 109.

12. Hasheminia, D., Razavi, S. M., Nazari, H., Khazaei, S., & Soleimanzadeh, P. Systemic supplement with resveratrol increased bone formation in ratsâ alveolar socket Aumento de la formaciÃ³n Ã³sea en el hueso alveolar de rata con suplemento sistÃ© mico con resveratrol. International Journal of Morphology, 2018, 36(2), 391-394.

13. Gao, C., Feng, P., Peng, S., & Shuai, C. Carbon nanotube, graphene and boron nitride nanotube reinforced bioactive ceramics for bone repair. Acta biomaterialia, 2017, 61, 1-20.

14. Shuai, C., Gao, C., Feng, P., & Peng, S. Graphene-reinforced mechanical properties of calcium silicate scaffolds by laser sintering. RSC Advances, 2014, 4(25), 12782-12788.

15. White, A. A., Best, S. M., & Kinloch, I. A. Hydroxyapatite–carbon nanotube composites for biomedical applications: a review. International Journal of Applied Ceramic Technology, 2007, 4(1), 1-13.

16. Touri, R., Moztarzadeh, F., Sadeghian, Z., Bizari, D., Tahriri, M., & Mozafari, M. The use of carbon nanotubes to reinforce 45S5 bioglass-based scaffolds for tissue engineering applications. BioMed research international, 2013.

17. Burg, K. J., Porter, S., & Kellam, J. F. Biomaterial developments for bone tissue engineering. Biomaterials, 2000, 21(23), 2347-2359.

18. Dorozhkin, S. V., & Epple, M. Biological and medical significance of calcium phosphates. Angewandte Chemie International Edition, 2002, 41(17), 3130-3146.

19. Sahmani, S., Shahali, M., Nejad, M. G., Khandan, A., Aghdam, M. M., & Saber-Samandari, S. Effect of copper oxide nanoparticles on electrical conductivity and cell viability of calcium phosphate scaffolds with improved mechanical strength for bone tissue engineering. The European Physical Journal Plus, 2019, 134(1), 7.

20. Khandan, A., Karamian, E., & Bonakdarchian, M. Mechanochemical synthesis evaluation of nanocrystalline bone-derived bioceramic powder using for bone tissue engineering. Dental Hypotheses, 2014, 5(4), 155.

21. Abdellahi, M., Najafinezhad, A., Ghayour, H., Saber-Samandari, S., & Khandan, A. Preparing diopside nanoparticle scaffolds via space holder method: Simulation of the compressive strength and porosity. Journal of the Mechanical Behavior of Biomedical Materials, 2017, 72, 171-181.

22. Sahmani, S., Saber-Samandari, S., Shahali, M., Yekta, H. J., Aghadavoudi, F., Montazeran, A. H., … & Khandan, A. Mechanical and biological performance of axially loaded novel bio-nanocomposite sandwich plate-type implant coated by biological polymer thin film. Journal of the mechanical behavior of biomedical materials, 2018, 88, 238-250.

23. Yoshikawa, H., & Myoui, A. Bone tissue engineering with porous hydroxyapatite ceramics. Journal of Artificial Organs, 2005, 8(3), 131-136.

24. Jones, J. R., Gentleman, E., & Polak, J. Bioactive glass scaffolds for bone regeneration. Elements, 2007, 3(6), 393-399.

25. Gerhardt, L. C., & Boccaccini, A. R. Bioactive glass and glass-ceramic scaffolds for bone tissue engineering. Materials, 2010, 3(7), 3867-3910.

26. Aghdam, H. A., Sheikhbahaei, E., Hajihashemi, H., Kazemi, D., & Andalib, A. The impacts of internal versus external fixation for tibial fractures with simultaneous acute compartment syndrome. European Journal of Orthopaedic Surgery & Traumatology, 2019, 29(1), 183-187.

27. Tahririan, M. A., Motififard, M., Omidian, A., Aghdam, H. A., & Esmaeali, A. Relationship between bone mineral density and serum vitamin D with low energy hip and distal radius fractures: A case-control study. Archives of Bone and Joint Surgery, 2017, 5(1), 22.

28. Esmaeili, S., Aghdam, H. A., Motififard, M., Saber-Samandari, S., Montazeran, A. H., Bigonah, M.,. & Khandan, A. A porous polymeric–hydroxyapatite scaffold used for femur fractures treatment: fabrication, analysis, and simulation. European Journal of Orthopaedic Surgery & Traumatology, 2020, 30(1), 123-131.

29. Pemmer, B., Roschger, A., Wastl, A., Hofstaetter, J. G., Wobrauschek, P., Simon, R., & Streli, C. Spatial distribution of the trace elements zinc, strontium and lead in human bone tissue. Bone, 2013, 57(1), 184-193.

30. Bagherifard, A., Joneidi Yekta, H., Akbari Aghdam, H., Motififard, M., Sanatizadeh, E., Ghadiri Nejad, M., & Khandan, A. Improvement in osseointegration of tricalcium phosphate-zircon for orthopedic applications: an in vitro and in vivo evaluation. Medical & Biological Engineering & Computing, 2020, 58, 1681-1693.

31. Aghdam, H. A., Sanatizadeh, E., Motififard, M., Aghadavoudi, F., Saber-Samandari, S., Esmaeili, S., & Khandan, A. Effect of calcium silicate nanoparticle on surface feature of calcium phosphates hybrid bio-nanocomposite using for bone substitute application. Powder Technology, 2020, 361, 917-929.

32. Xu, S., Lin, K., Wang, Z., Chang, J., Wang, L., Lu, J., & Ning, C. Reconstruction of calvarial defect of rabbits using porous calcium silicate bioactive ceramics. Biomaterials, 2008, 29(17), 2588-2596.

33. Lin, K., Xia, L., Li, H., Jiang, X., Pan, H., Xu, Y., & Chang, J. Enhanced osteoporotic bone regeneration by strontium-substituted calcium silicate bioactive ceramics.

Biomaterials, 2013, 34(38), 10028-10042.

34. Mehrali, M., Moghaddam, E., Shirazi, S. F. S., Baradaran, S., Mehrali, M., Latibari, S. T., & Osman, N. A. A. Synthesis, mechanical properties, and in vitro biocompatibility with osteoblasts of calcium silicate–reduced graphene oxide composites. ACS applied materials & interfaces, 2014, 6(6), 3947-3962.

35. Shao, H., He, Y., Fu, J., He, D., Yang, X., Xie, J., & Gou, Z. 3D printing magnesium-doped wollastonite/β-TCP bioceramics scaffolds with high strength and adjustable degradation. Journal of the European Ceramic Society, 2016, 36(6), 1495-1503.

36. Saravanan, S., Nethala, S., Pattnaik, S., Tripathi, A., Moorthi, A., & Selvamurugan, N. Preparation, characterization and antimicrobial activity of a bio-composite scaffold containing chitosan/nano-hydroxyapatite/ nano-silver for bone tissue engineering. International journal of biological macromolecules, 2011, 49(2), 188-193.

37. Raisi, A., Asefnejad, A., Shahali, M., Doozandeh, Z., Kamyab Moghadas, B., Saber-Samandari, S., & Khandan, A. A soft tissue fabricated using freeze-drying technique with carboxymethyl chitosan and nanoparticles for promoting effects on wound healing. Journal of Nanoanalysis, 2020.

38. Sahmani, S., Khandan, A., Saber-Samandari, S., & Aghdam, M. M. Effect of magnetite nanoparticles on the biological and mechanical properties of hydroxyapatite porous scaffolds coated with ibuprofen drug. Materials Science and Engineering: C, 2020, 110835.

39. Lee, H., Kim, Y., Kim, S., & Kim, G. Mineralized biomimetic collagen/alginate/silica composite scaffolds fabricated by a low-temperature bio-plotting process for hard tissue regeneration: fabrication, characterisation and in vitro cellular activities. Journal of Materials Chemistry B, 2014, 2(35), 5785-5798.

40. A Ghadirinejad, M., Atasoylu, E., Izbirak, G., & GHA-SEMI, M. A stochastic model for the ethanol pharmacokinetics. Iranian journal of public health, 2016, 45(9), 1170.

41. Ramanathan, G., Singaravelu, S., Raja, M. D., Nagiah, N., Padmapriya, P., Ruban, K., &

73

Perumal, P. T. Fabrication and characterization of a collagen coated electrospun poly (3-hydroxybutyric acid)–gelatin nanofibrous scaffold as a soft bio-mimetic material for skin tissue engineering applications. RSC Advances, 2016, 6(10), 7914-7922.

42. Sahmani, S., Khandan, A., Esmaeili, S., Saber-Samandari, S., Nejad, M. G., & Aghdam, M. M. Calcium phosphate-PLA scaffolds fabricated by fused deposition modeling technique for bone tissue applications: fabrication, characterization and simulation. Ceramics International, 2020, 46(2), 2447-2456.

43. Xiong, G., Luo, H., Zuo, G., Ren, K., & Wan, Y. Novel porous graphene oxide and hydroxyapatite nanosheets-reinforced sodium alginate hybrid nanocomposites for medical applications. Materials Characterization, 2015, 107, 419-425.

44. Karkeh-abadi, F., Saber-Samandari, S., & Saber-Samandari, S. The impact of functionalized CNT in the network of sodium alginate-based nanocomposite beads on the removal of Co (II) ions from aqueous solutions. Journal of hazardous materials, 2016, 312, 224-233.

45. Ionita, M., Pandele, M. A., & Iovu, H. Sodium alginate/graphene oxide composite films with enhanced thermal and mechanical properties. Carbohydrate polymers, 2013, 94(1), 339-344.

46. Sin, D., Miao, X., Liu, G., Wei, F., Chadwick, G., Yan, C., & Friis, T. Polyurethane (PU) scaffolds prepared by solvent casting/particulate leaching (SCPL) combined with centrifugation. Materials Science and Engineering: C, 2010, 30(1), 78-85.

47. Liao, C. J., Chen, C. F., Chen, J. H., Chiang, S. F., Lin, Y. J., & Chang, K. Y. Fabrication of porous biodegradable polymer scaffolds using a solvent merging/particulate leaching method. Journal of Biomedical Materials Research: An Official Journal of The Society for Biomaterials, The Japanese Society for Biomaterials, and The Australian Society for Biomaterials and the Korean Society for Biomaterials, 2002, 59(4), 676-681.

48. Saber-Samandari, S., & Gross, K. A. Nano-indentation on amorphous calcium phosphate splats: Effect of droplet size on mechanical

properties. Journal of the mechanical behavior of biomedical materials, 2012, 16, 29-37.

49. Liu, X., & Ma, P. X. Phase separation, pore structure, and properties of nanofibrous gelatin scaffolds. Biomaterials, 2009, 30(25), 4094-4103.

50. [50] Abd-Khorsand, S., Saber-Samandari, S., & Saber-Samandari, S. Development of nanocomposite scaffolds based on TiO2 doped in grafted chitosan/hydroxyapatite by freeze drying method and evaluation of biocompatibility. International journal of biological macromolecules, 2017, 101, 51-58.

51. Sahmani, S., Shahali, M., Khandan, A., Saber-Samandari, S., & Aghdam, M. M. Analytical and experimental analyses for mechanical and biological characteristics of novel nanoclay bio-nanocomposite scaffolds fabricated via space holder technique. Applied Clay Science, 2018, 165, 112-123.

52. Kordjamshidi, A., Saber-Samandari, S., Nejad, M. G., & Khandan, A. Preparation of novel porous calcium silicate scaffold loaded by celecoxib drug using freeze drying technique: Fabrication, characterization and simulation. Ceramics International, 2019, 45(11), 14126-14135.

53. Khandan, A., Saber-Samandari, S., Telloo, M., Kazeroni, Z. S., Esmaeili, S., Sheikhbahaei, E., ... & Kamyab, B. A Mitral Heart Valve Prototype Using Sustainable Polyurethane Polymer: Fabricated by 3D Bioprinter, Tested by Molecular Dynamics Simulation. AUT Journal of Mechanical Engineering, 2020.

54. Kulkarni, P., Rawtani, D., & Barot, T. Formulation and optimization of long acting dual niosomes using box-Behnken experimental design method for combinative delivery of ethionamide and D-cycloserine in tuberculosis treatment. Colloids and Surfaces A: Physicochemical and Engineering Aspects, 2019, 565, 131-142.

55. Barot, T., Rawtani, D., Kulkarni, P., Hussain, C. M., & Akkireddy, S. Physicochemical and biological assessment of flowable resin composites incorporated with farnesol loaded halloysite nanotubes for dental applications. Journal of the Mechanical Behavior of Biomedical Materials, 2020, 104, 103675.

56. Barot, T., Rawtani, D., & Kulkarni, P. Physicochemical and biological assessment of

silver nanoparticles immobilized Halloysite nanotubes-based resin composite for dental applications. Heliyon, 2020, 6(3), e03601.

57. Barot, T., Rawtani, D., & Kulkarni, P. Development of Chlorhexidine Loaded Halloysite Nanotube Based Experimental Resin Composite with Enhanced Physico-Mechanical and Biological Properties for Dental Applications. Journal of Composites Science, 2020, 4(2), 81.

58. Patel, P., Barot, T., & Kulkarni, P. Formulation, Characterization and In-vitro and In-vivo Evaluation of Capecitabine Loaded Niosomes. Current Drug Delivery, 2020, 17(3), 257-268.

59. Foroutan, S., Hashemian, M., Khandan, A. A Porous Sodium Alginate-CaSiO₃ Polymer Reinforced with Graphene Nanosheet: Fabrication and Optimality Analysis: Fibers and Polymers, 2020.

60. Saber-Samandari, S., Saber-Samandari, S., Ghonjizade-Samani, F., Aghazadeh, J., & Sadeghi, A. Bioactivity evaluation of novel nanocomposite scaffolds for bone tissue engineering: The impact of hydroxyapatite. Ceramics International, 2016, 42(9), 11055-11062.

61. Sahmani, S., Khandan, A., Saber-Samandari, S., & Aghdam, M. M. Nonlinear bending and instability analysis of bioceramics composed with magnetite nanoparticles: Fabrication, characterization, and simulation. Ceramics International, 2018, 44(8), 9540-9549.

62. [62] Foroutan, S., Haghshenas, A., Hashemian, M., Eftekhari, S. A., & Toghraie, D. Spatial buckling analysis of current-carrying nanowires in the presence of a longitudinal magnetic field accounting for both surface and nonlocal effects. Physica E: Low-Dimensional Systems and Nanostructures, 2018, 97, 191-205.

63. Shu, C. Differential quadrature and its application in engineering. Springer Science & Business Media., 2012, 26-38.

64. Torkan, E., Pirmoradian, M., & Hashemian, M. Instability inspection of parametric vibrating rectangular Mindlin plates lying on Winkler foundations under periodic loading of moving masses. Acta Mechanica Sinica, 2019, 35(1), 242-263.

65. Salmani, M. M., Hashemian, M., Yekta, H.

J., Nejad, M. G., Saber-Samandari, S., & Khandan, A. Synergic Effects of Magnetic Nanoparticles on Hyperthermia-Based Therapy and Controlled Drug Delivery for Bone Substitute Application. JOURNAL OF SUPERCONDUCTIVITY AND NOVEL MAGNETISM, 2020. 33, 2809-2820.

66. Wagner, G. J., & Liu, W. K. Application of essential boundary conditions in mesh-free methods: a corrected collocation method. International Journal for Numerical Methods in Engineering, 2000, 47(8), 1367-1379.

67. Aghadavoudi, F., Golestanian, H., & Beni, Y. T. Investigation of cnt defects on mechanical behavior of cross linked epoxy based nanocomposites by molecular dynamics. Int J Adv Design Manuf Technol, 2016, 9(1), 137-146.

68. Farazin, A., Aghadavoudi, F., Motififard, M., Saber-Samandari, S., & Khandan, A. Nanostructure, molecular dynamics simulation and mechanical performance of PCL membranes reinforced with antibacterial nanoparticles. Journal of Applied and Computational Mechanics, 2020.

69. Kamarian, S., Bodaghi, M., Isfahani, R. B., & Song, J. A comparison between the effects of shape memory alloys and carbon nanotubes on the thermal buckling of laminated composite beams. Mechanics Based Design of Structures and Machines, 2020.

70. Kamarian, S., Bodaghi, M., Isfahani, R. B., & Song, J. Thermal buckling analysis of sandwich plates with soft core and CNT-reinforced composite face sheets. Journal of Sandwich Structures and Materials, 2020.

71. Moeini, M., Barbaz Isfahani, R., Saber-Samandari, S., & Aghdam, M. M. Molecular dynamics simulations of the effect of temperature and strain rate on mechanical properties of graphene–epoxy nanocomposites. Molecular Simulation, 2020, 46(6), 476-486.

72. Kamarian, S., Bodaghi, M., Isfahani, R. B., Shakeri, M., & Yas, M. H. Influence of carbon nanotubes on thermal expansion coefficient and thermal buckling of polymer composite plates: Experimental and numerical investigations. Mechanics Based Design of Structures and Machines, 2019, 1-16.

73. Maghsoudlou, M. A., Isfahani, R. B., Saber-Samandari, S., & Sadighi, M. Effect of

75

interphase, curvature and agglomeration of SWCNTs on mechanical properties of polymer-based nanocomposites: Experimental and numerical investigations. Composites Part B: Engineering, 2019, 175, 107119.

74. Maghsoudlou, M. A., Nassireslami, E., Saber-Samandari, S., & Khandan, A. Bone regeneration using bio-nanocomposite tissue reinforced with bioactive nanoparticles for femoral defect applications in medicine. Avicenna Journal of Medical Biotechnology, 2020, 12(2), 68.

75. Amini, E., Nassireslami, E., Payandemehr, B., Khodagholi, F., Foolad, F., Khalaj, S., & Sharifzadeh, M. Paradoxical role of PKA inhibitor on amyloidβ-induced memory deficit. Physiology & Behavior, 2015, 149, 76-85.

76. Seyedi, S. Y., Salehi, F., Payandemehr, B., Hossein, S., Hosseini-Zare, M. S., Nassireslami, E., & Sharifzadeh, M. Dual effect of cAMP agonist on ameliorative function of PKA inhibitor in morphine-dependent mice. Fundamental & clinical pharmacology, 2014, 28(4), 445-454.

77. Baradaran, S., Nasiri-Tabrizi, B., Shirazi, F. S., Saber-Samandari, S., Shahtalebi, S., & Basirun, W. J. Wet chemistry approach to the preparation of tantalum-doped hydroxyapatite: Dopant content effects. Ceramics International, 2018, 44(3), 2768-2781.

78. Nassireslami, E., & Ajdarzade, M. Gold coated superparamagnetic iron oxide nanoparticles as effective nanoparticles to eradicate breast cancer cells via photothermal therapy. Advanced pharmaceutical bulletin, 2018, 8(2), 201-209.